

Challenges in molecular dynamics simulations of heat exchange statistics

Jonathan J. Wang,¹ Matthew Gerry,² and Dvira Segal^{1,2}

¹*Chemical Physics Theory Group, Department of Chemistry, University of Toronto, 80 Saint George St., Toronto, Ontario M5S 3H6, Canada*

²*Department of Physics, University of Toronto, 60 Saint George St., Toronto, Ontario M5S 1A7, Canada*

(*Electronic mail: dvira.segal@utoronto.ca)

(Dated: November 15, 2023)

We study heat exchange in temperature-biased metal-molecule-metal molecular junctions by employing the LAMMPS atomic molecular dynamics simulator. Generating the nonequilibrium steady state with Langevin thermostats at the boundaries of the junction, we show that the *average* heat current across a gold-alkanedithiol-gold nanojunction behaves correctly-physically, with the thermal conductance value matching the literature. In contrast, the *full probability distribution function* for heat exchange, as generated by the simulator, violates the fundamental fluctuation symmetry for entropy production. We trace this failure back to the implementation of the thermostats and the expression used to calculate the heat exchange. To rectify this issue and produce the correct statistics, we introduce single-atom thermostats as an alternative to conventional many-atom thermostats. Once averaging heat exchange over the hot and cold thermostats, this approach successfully generates the correct probability distribution function, which we use to study the behavior of both the average heat current and its noise. We further examine the thermodynamic uncertainty relation in the molecular junction and show that it holds, albeit demonstrating nontrivial trends. Our study points to the need to carefully implement nonequilibrium molecular dynamics solvers in atomistic simulation software tools for future investigations of noise phenomena in thermal transport.

I. INTRODUCTION

Nanoscale thermal transport has been increasingly studied in relation to different applications, including electronics, thermoelectrics, and plasmonics¹⁻¹⁰. Considering molecular-based technologies, recent experiments have focused on characterizing and elucidating thermal transport mechanisms in self-assembled monolayers (SAMs)¹¹⁻¹⁶ and single-molecule junctions¹⁷⁻¹⁹. Focusing on the latter, it is important to recognize that the instrumentation involved is highly challenging due to the minuscule currents at play. For instance, heat currents measured in single alkane junctions are in the picowatts range; such measurements are done by reading electronic probes acting at the interface, rather than within the molecule itself¹⁷.

Studies of thermal transport in single molecules provide fundamental understanding on transport mechanisms as well as guidelines for advancing energy technologies. However, due to the experimental challenge involved in such studies, simulations play a central role in supporting and directing experiments. In this context, classical molecular dynamics (MD) simulations stand out as a practical and reasonably accurate tool for characterizing thermal transport behavior, especially at elevated temperatures. Although these simulations are obviously approximate in modelling interactions between atoms, compared to first-principle based approaches, the use of empirical potentials significantly reduces computational demands and allow probing questions such as how the introduction of many body effects allow the transition from anomalous to normal conduction^{20,21}.

Given their structural simplicity, thermal transport in gold-alkanedithiol-gold single-molecule junctions has been examined in detail both experimentally¹⁷⁻¹⁹ and computationally²²⁻³². Notably, simulations of thermal con-

ductance of these systems showed that transport was ballistic (non-dissipative) thus approximately length-independent, in good agreement with experimental results.

Nonequilibrium atomistic MD simulations of heat transport have been traditionally focused on the analysis of the average heat current passing through the junction. In contrast, investigations of *full counting statistics* have been confined to simplistic one-dimensional model systems of beads and springs³³⁻⁴¹. Identifying this gap, our objective in this paper is to explore the full probability distribution function of heat exchange, $P(Q_\tau)$ within a detailed, experimentally relevant atomistic model of a thermal transport junction, as illustrated in Fig. 1. Here, Q_τ is defined as the net heat exchange between the hot reservoir and the system within a time τ ; one can also calculate the corresponding heat exchange at the cold end. τ stands for a time interval long enough to eliminate dependence on initial conditions.

Our motivation for studying the properties of $P(Q_\tau)$ is twofold. Primarily, this would allow testing and improving the simulation algorithm through the verification of the heat exchange fluctuation theorem, which holds in nonequilibrium steady state³³⁻⁴¹,

$$\frac{P(Q_\tau)}{P(-Q_\tau)} = e^{\Delta\beta Q_\tau}, \quad (1)$$

Here, $\Delta\beta \equiv \frac{1}{k_B} \left(\frac{1}{T_{\text{cold}}} - \frac{1}{T_{\text{hot}}} \right)$ is the difference between the inverse temperatures of the two electrodes with k_B as the Boltzmann's constant (a more precise discussion of $\Delta\beta$ is included in Sec. II). $\Delta\beta Q_\tau$ is the entropy production in the reservoirs during time τ . Eq. (1) is a special case of the more general statement on the symmetry of entropy production in nonequilibrium steady state, leading to the second law of thermodynamics³³⁻⁴⁰. Confirming the validity of the relation (1) through simulations serves to attest that the simula-

tion method generates data which obeys physical principles. This in turn enables the investigation of the nature of fluctuations and their influence on the operation of thermal devices, which is our second motivation for studying the behavior of this distribution function. While such investigations were carried out on model systems such as the nonequilibrium spin-boson model^{42–50}, simulations of heat current fluctuations in detailed atomistic nanojunctions are lacking.

In particular, cost (dissipation) - precision (noise) trade-offs in nanoscale systems gained enormous interest in the last decade^{51–60}. The thermodynamic uncertainty relation (TUR) was proved for continuous-time Markov state processes⁵², and subsequently for overdamped Langevin dynamics^{54,55}. However, the original TUR does not universally hold under underdamped Langevin dynamics⁵⁸. The study of nonequilibrium noise in molecular junctions and the analysis of the TUR beyond overdamped dynamics hold significance both from a fundamental perspective and for applications.

In this work, we study heat exchange within a gold-alkanedithiol-gold single-molecule junction using classical MD simulations. We begin by employing the standard procedure of nonequilibrium molecular dynamics (NEMD) simulations as implemented in the LAMMPS software. Our work reveals that the conventional approach of utilizing many-atom Langevin thermostats at the boundaries of the junction results in a distribution function $P(Q_\tau)$ that fails to satisfy the fluctuation theorem for heat exchange. While the NEMD method correctly provides the average heat current, it does not capture the correct statistical behavior of heat fluctuations.

Several algorithmic issues contribute to this discrepancy, including the adoption of a problematic definition for heat exchange⁴¹ and the use of deterministic solvers for differential equations, instead of stochastic solvers. Notably, our analysis identifies the application of many-atom thermostats as another significant contributor to the breakdown of the fluctuation symmetry. As such, in the second part of the paper we introduce *single-atom thermostats*, which thermalize a single atom at each boundary. This setup rectifies the statistics, leading to distribution functions $P(Q_\tau)$ that satisfy the fluctuation symmetry. Importantly, we confirm that our modified thermostat approach delivers the correct thermal conductance coefficient and produces physical temperature profiles. We also study the current noise and observe nontrivial and nonmonotonic behavior in the TUR ratio. These findings will guide measurements of full counting statistics of heat exchange in single-molecule thermal junctions.

The paper is organized as follows. In Sec. II we outline the NEMD simulation methodology and explain the analysis required to build the distribution function $P(Q_\tau)$. We present results from simulations in two sections: In Sec. III, we discuss calculations of the full probability distribution function for heat exchange when using conventional many-atom thermostats, demonstrating violations to the fluctuation symmetry. This deficiency is addressed and resolved in Sec. IV, by implementing single-atom thermostats. We summarize our work in Sec. V and discuss potential future directions.

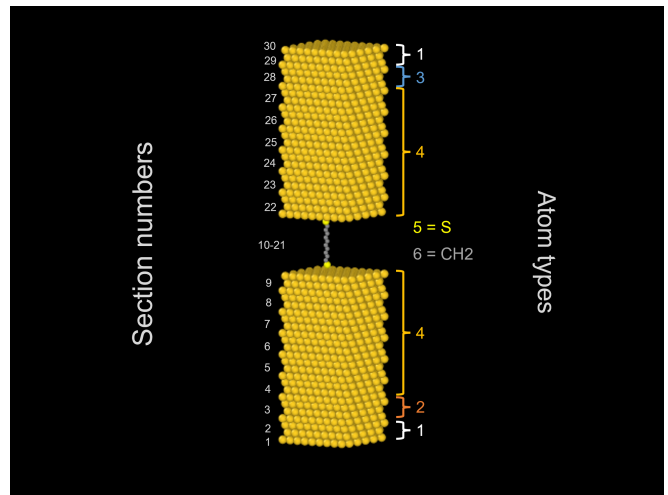


Figure 1. **Visualization of the system simulated in this work** (OVITO program⁶²). The setup includes two Au metals with 2160 atoms each, connected by an alkanedithiol molecule with 10 carbon atoms. In this setup, Langevin baths are enacted close to the ends of Au leads, away from the conducting molecule. Atom types appearing at the right side distinguishes between regions of Au leads as well as the molecule as defined in LAMMPS. Type 1 atoms are fixed Au atoms that hold the system in place (270 atoms at each side). Type 2 and 3 atoms are Au regions that are thermostated with hot and cold baths, respectively (270 atoms at each side). Type 4 atoms encompass the remaining moving Au atoms. Type 5 and 6 atoms comprise the single alkane molecule, distinguishing between the S and the unified CH₂ atoms. Section numbers (left) denote regions over which temperature is averaged to produce the simulation temperature profile.

II. SETUP AND SIMULATION TECHNIQUE

A. Setup and procedure

We study heat transfer through a single molecule positioned between gold leads, as illustrated in Fig. 1. In our work, we ignore the direct electronic contribution to heat flow, and focus on the phononic-vibrational contribution to it. Since we take into account interatomic interactions beyond the harmonic force field, we rely on classical MD as our tool of choice.

Our primary objectives are to produce MD data for molecular junctions consistent with the heat exchange fluctuation symmetry, and use it to study the heat current and its fluctuations. As such, the specific molecule chosen is not critical to our investigation. Given that notable experimental studies have focused on thermal transport within alkane chains^{17,18}, we have opted in our study to employ an alkanedithiol molecule with 10 carbon atoms.

We carry out simulations using the Large-scale Atomic/Molecular Massively Parallel Simulator⁶¹ (LAMMPS), and we visualize the system through OVITO⁶². To study phononic-vibrational heat transport, we employ the NEMD simulation approach. In this method, a temperature bias is imposed through the boundaries, and it induces a net

heat current across the junction. The gold-alkanedithiol-gold system setup and the empirical interatomic potentials utilized were described in detail in Ref. 31. Briefly, before the production run, the system undergoes equilibration in the NPT then NVT ensembles to attain zero pressure and to reach a target temperature \bar{T} . During the NVE simulation production run, Langevin thermostats are applied to opposite segments of the gold, one set at the high temperature T_{hot} , the other at the low temperature T_{cold} , with the imposed bias $\Delta T = T_{\text{hot}} - T_{\text{cold}}$.

Specifically, the gold atoms that are coupled to the baths follow the Langevin equation of motion, which ensures controlled temperature conditions in that boundary, $m_{\text{Au}} \frac{d\vec{v}_n}{dt} = \vec{F}_n(t) - \gamma m_{\text{Au}} \vec{v}_n + \vec{\xi}_n(t)$. Here, \vec{F}_n is the deterministic force acting on atom n , derived from the interatomic potentials at time t . \vec{v}_n is the velocity vector of atom n with mass m_{Au} . As for the Langevin terms, γ is the friction, or damping coefficient (dimension of inverse time) and $\vec{\xi}_n(t)$ is a Gaussian stochastic force applied to the n th atom with a delta-time correlation function, $\langle \xi_{n,j}(t) \xi_{n,k}(t') \rangle = 2\gamma k_B T m_{\text{Au}} \delta(t-t') \delta_{k,j}$; T is the temperature of the thermostat and k, j refer to the different spatial coordinates for each atom n . Input parameters to this simulation are the temperatures T_{hot} and T_{cold} and the damping rate γ . In our simulations, we employed a timestep $\Delta t = 1$ fs and performed production simulations over a total simulation time ranging from 10 ns (for studying thermal conductance) to 50 ns (for conducting fluctuation analysis).

The instantaneous heat current at the hot side is given by

$$J_{\text{hot}}(t) = -\gamma \sum_n \sum_{j=x,y,z} \frac{[p_{n,j}(t)]^2}{m_{\text{Au}}} + \frac{1}{m_{\text{Au}}} \sum_n \sum_{j=x,y,z} \xi_{n,j}(t) p_{n,j}(t), \quad (2)$$

where the sum is performed over all degrees of freedom that are being thermostated, with n an atom index and $j = x, y, z$ the direction. Here, $p_{n,j}(t)$ is the momentum of a particle and $\xi_{n,j}(t)$ the applied random force. A similar expression can be written to calculate the instantaneous heat current at the cold end, J_{cold} . The cumulative heat exchange is obtained by summing up the heat current over a certain interval. For example, the amount of heat exchange with the hot Langevin bath is

$$Q_{\tau}^{\text{hot}} = \int_{\tau_0}^{\tau_0+\tau} J_{\text{hot}}(t) dt. \quad (3)$$

Here, τ_0 is selected after the nonequilibrium steady state sets in. Our sign convention is such that heat input from the hot Langevin bath to the thermostated atoms is defined as positive. As for the cold reservoir, we use the opposite sign convention.

B. Data analysis

The output data from LAMMPS provides us with the *cumulative* energy absorbed by the system from the hot and cold Langevin thermostats, separately. This data is collected as a function of time⁶¹. We denote the total energy exchange

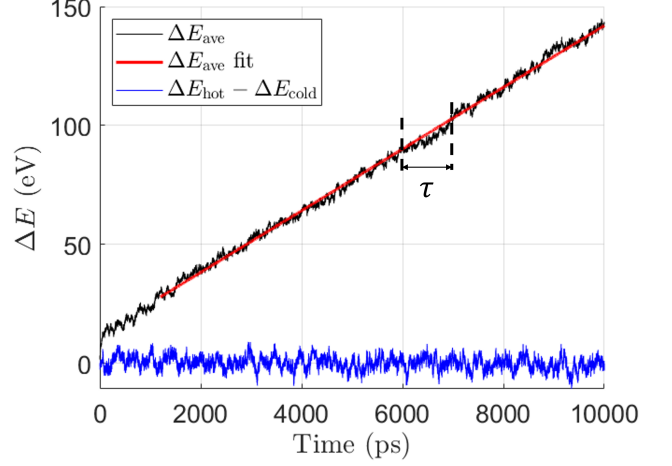


Figure 2. **Cumulative energy exchange of the system with the Langevin thermostats presented as a function of time.** $\Delta E_{\text{ave}}(t)$ is the average of $\Delta E_{\text{hot}}(t)$ and $\Delta E_{\text{cold}}(t)$; the full red line represents a linear fit from which the current J is extracted. An example of the definition of integration time interval τ is shown. In this plot, τ is approximately 1000 ps, and the difference between ΔE values at the dashed lines give Q_{τ} . We additionally display energy conservation in our simulated system with $\Delta E_{\text{hot}}(t) - \Delta E_{\text{cold}}(t)$. Simulation parameters are $\bar{T} = 300$ K, $\Delta T = 50$ K, $\gamma^{-1} = 0.04$ ps.

with the hot and cold thermostats up to time t by $\Delta E_{\text{hot}}(t)$ and $\Delta E_{\text{cold}}(t)$, respectively, where, e.g., $\Delta E_{\text{hot}}(t) = \int_0^t J_{\text{hot}}(t') dt'$. In the steady state limit, the time-averaged energy emitted from the hot bath should be equal to the energy absorbed by the cold bath. Indeed, as seen in Fig. 2, the difference $\Delta E_{\text{hot}}(t) - \Delta E_{\text{cold}}(t)$ hovers around zero, in line with expectations (recall our sign convention, given below Eq. (3)). Furthermore, in steady state the averaged heat current across the junction can be calculated equivalently at either contact as $J_{\text{hot}} = \frac{\Delta E_{\text{hot}}(t)}{t}$, $J_{\text{cold}} = \frac{\Delta E_{\text{cold}}(t)}{t}$, as well as from their average $J_{\text{ave}} = \frac{\Delta E_{\text{ave}}(t)}{t}$, where $\Delta E_{\text{ave}}(t) = \frac{\Delta E_{\text{hot}}(t) + \Delta E_{\text{cold}}(t)}{2}$. In Fig. 2, we display the cumulative energy exchange $\Delta E_{\text{ave}}(t)$ as a function of time. As expected, it grows linearly in time, and we extract the heat current as the slope of this curve.

The thermal conductance of the junction, denoted by G , is defined from the relationship $J = G \Delta T_{\text{Au-Au}}$. Here J stands for the current, which can be evaluated at either contacts, or computed from the average, with $\Delta T_{\text{Au-Au}}$ representing the actual temperature difference between the metals. We present such simulations in Fig. 3 (discussed in details in Sec. III). In Ref. 31, we discussed both the molecular conductance and the junction's conductance.

The role of the thermostats is to drive the two different metals towards distinct temperatures, T_{hot} and T_{cold} . We define $\Delta T = T_{\text{hot}} - T_{\text{cold}}$ as the *imposed* temperature difference. We further introduce two other measures for our analysis. As mentioned above, $\Delta T_{\text{Au-Au}}$ stands for the temperature difference as observed on gold atoms located at the gold layer closest to the molecule. This bias serves to calculate the thermal conductance of the *junction*. We assess the fluctuation sym-

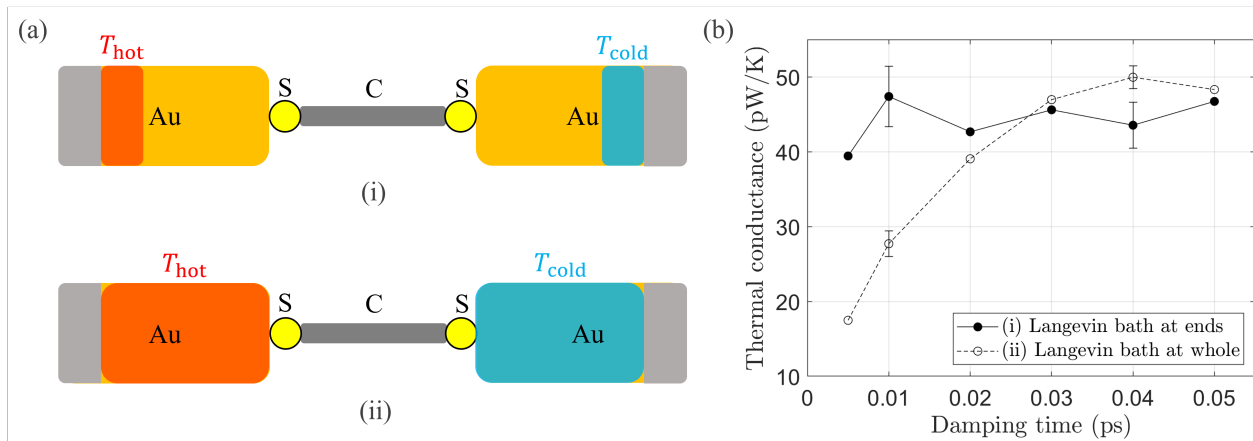


Figure 3. **Nonequilibrium molecular dynamics simulations with different many-atom Langevin thermostats at the two ends.** (a) Each (cold, hot) thermostat either apply to (i) only a certain region of the metal further away from the molecule or to (ii) all moving Au atoms. The light gray blocks at the ends indicate fixed Au that hold the system in place. (b) The resulting thermal conductance as a function of Langevin damping time parameter, the inverse of γ in the Langevin equation. The temperatures are set with $\bar{T} = 300$ K, $\Delta T = 50$ K. For $\gamma^{-1} = 0.01$ and 0.04 ps we performed each calculation three times and the error bars reflect the standard deviation of results.

metry in relation to this temperature bias, which in practice is very close to the imposed bias ΔT . Additionally, ΔT_{S-S} quantifies the temperature difference observed between the two sulfur atoms situated at the edges of the carbon chain. Unlike ΔT_{Au-Au} , which pertains to the metal-molecule-metal junction, ΔT_{S-S} is used to calculate the thermal conductance of the molecule itself. We illustrate and discuss these temperature biases below in Fig. 4(a).

The cumulative heat exchange data collected is used to generate the full probability distribution of heat exchange, for testing the steady state heat exchange fluctuation symmetry (1) and calculating cumulants of the current⁴¹. Using simulation data, we generate the ensemble of heat exchange values during time interval τ . For example, for the hot side $Q_{\tau}^{\text{hot},(i)} = \Delta E_{\text{hot}}(t_i + \tau) - \Delta E_{\text{hot}}(t_i)$. We generate three such sets based on heat exchanged at the cold and hot baths, as well as when using the averaged heat exchanged $\Delta E_{\text{ave}}(t)$, to yield Q_{τ}^{cold} , Q_{τ}^{hot} , and Q_{τ}^{ave} , respectively. For these three ensembles we generate histograms of the heat exchange, $P(Q_{\tau})$, and test the fluctuation symmetry, Eq. (1). Such results are presented in Fig. 5 for the many-atom thermostats. We turn to single-atom thermostats in Fig. 6. We present the histogram of the heat exchange in Fig. 7 and we use the probability distribution of heat exchange to compute the current noise and the TUR in Fig. 8. As for the values of $\Delta\beta$ in Eq. (1), rather than substituting the thermostats' target temperatures, T_{hot} and T_{cold} , we use here the actual steady state temperatures developing at the metal right next to the molecule.

III. CONVENTIONAL MANY-ATOM THERMOSTATS

A. Average heat current

We begin with the calculation of the thermal conductance G through NEMD simulations. In a previous study³¹,

we tested two methodologies for assessing thermal transport within junctions: The approach-to-equilibrium MD (AEMD) method, which extracts the thermal conductance from the equilibration dynamics⁶³, and the reversed NEMD (RNEMD) method, where we impose the steady state current passing through the junction, and recover the internal temperature bias^{15,16,23,64}. In Ref. 31 we demonstrated that both methods provided results consistent with other studies and with experiments. The RNEMD method in particular came up as a robust tool. However, since the RNEMD method pins the heat current, it cannot be used to obtain the current fluctuations.

In the present work, however, we are interested in the statistics of heat exchange. As such, we have chosen to adopt a "direct" NEMD technique. In this method, the Langevin thermostats dictate the temperatures at the boundaries, and the heat current develops in accord. However, before proceeding to explore the heat exchange statistics, the method necessitates additional testings and verification. Two specific aspects of the method warrant examinations: (i) Determining the region of gold that should be subjected to thermalization. Intuitively, one would like to ensure that the region that is coupled to the bath is sufficiently distant from the junction of interest, thus avoiding interference of the Langevin thermostat with the actual phenomena under investigation. (ii) Optimizing the Langevin damping parameter γ . This thermostating parameter dictates the rate at which local thermal equilibrium is achieved. Striking the right balance is important: Small γ values lead to slow thermalization but minimize interference of the thermostat with the intrinsic dynamics. Large γ values accelerate thermalization, but at the potential cost of modifying the intrinsic system's behavior.

We examine both of these aspects in Fig. 3. We simulate two scenarios, as illustrated in Fig. 3(a): The Langevin baths are either coupled to the termini of the mobile Au segment (top) or they are connected to the entire moving Au atoms (bottom), as was done in e.g., Ref. 30. In both cases, we con-

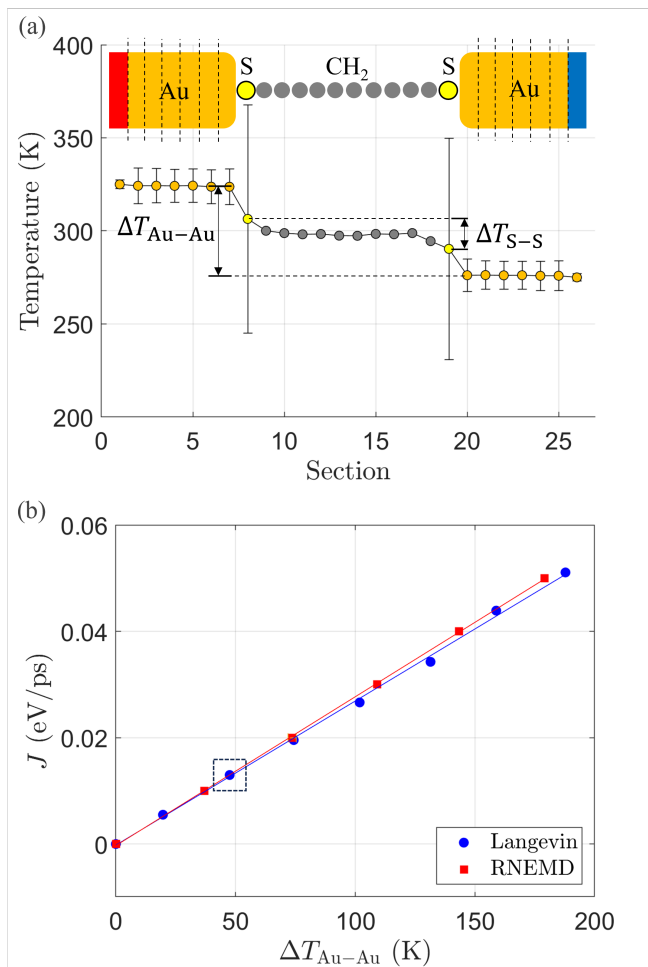


Figure 4. **Calculations of the heat current with different methods.** (a) An example of temperature profile generated on the junction in Langevin NEMD simulations. The imposed temperature difference is $\Delta T = 50$ K and we mark the generated biases, $\Delta T_{\text{Au-Au}}$ and $\Delta T_{\text{S-S}}$. The values of temperatures on Au and S atoms are shown along with their standard deviation. (b) Heat current J as a function of temperature difference of the junction $\Delta T_{\text{Au-Au}}$, comparing the Langevin NEMD (focus of this work) and RNEMD³¹ simulations. In both cases, we maintained $\bar{T} = 300$ K. The temperature profile for the data point highlighted by the dashed square appears in panel (a). For the Langevin NEMD simulations, a damping time $\gamma^{-1} = 0.04$ ps was applied. Simulations were repeated three times each. The size of the resulting error bars appear less than the size of markers.

duct simulations of the heat current, and we determine the thermal conductance of the junction by considering the temperatures taken from the slab of gold atoms closest to the junction.

Fig. 3(b) indicates that there is a significant difference between these two scenarios, depending on the value of the damping parameter. Note that the damping parameter, corresponding to the inverse of γ , is given here in units of time. A smaller value of the damping parameter signifies frequent interactions with the Langevin bath to regulate temperature, and vice versa⁶¹. When the damping time is short, having the

entire Au system coupled to baths (hot or cold) results in conductance that is dependent on γ (empty circles). This however is not desirable; the implementation of the thermostats should not affect the conduction of the junction. In contrast, we observe that the conductance remains independent of the application of the Langevin baths when they are applied only to the terminal regions of the gold (full circles).

Our calculation of the Au-alkanedithiol-Au system consistently results in thermal conductance of the junction of approximately 40-45 pW/K, in agreement with previous studies³¹. Notably, experiments have reported a smaller value in the range of 20 pW/K¹⁷.

Altogether, Fig. 3 shows that care needs to be exercised when employing Langevin baths in NEMD simulations for thermal transport. Moving forward, we have chosen to adopt the configuration with baths applied to the ends of the Au system (setup (i) in Fig. 3(a)). Additionally, we have selected a damping time of 0.04 ps as our optimal parameter for ongoing simulations.

To further examine our calculations, we simulate the heat current at various temperature biases using both the Langevin-based NEMD and the RNEMD method as described in Ref. 31. First, in Fig. 4(a) we illustrate the temperature profile generated in the Langevin-based NEMD method at $\Delta T = 50$ K. The temperature drops at the boundaries, while it is about constant in this quasi one-dimensional molecule. This indicates that the interfacial (molecule-metal) thermal resistance is the main obstacle to conduction in this junction⁹, while the molecule conducts approximately ballistically. Next, in Fig. 4(b) we show that both methods exhibit a linear relationship between the heat current and the temperature difference in the junction. This trend is expected for alkane chains, and the two methods follow each other well. Note that $\Delta T_{\text{Au-Au}}$ represents the steady state temperature difference on gold segments next to the molecule, differing marginally from the thermostat temperature difference, ΔT , as can be seen in Fig. 4(a). As a reminder, in the RNEMD method, the steady state temperature difference is deduced from the temperature profile that develops on the junction. In the present "direct" Langevin NEMD method, $\Delta T_{\text{Au-Au}} \leq \Delta T$; a small temperature gradient develops across the Au leads due to thermostats placed at the ends. The thermal conductance G can be extracted easily from the current-bias slope to be 43.4 and 44.8 pW/K for the NEMD and RNEMD methodologies, respectively.

B. Fluctuations

We explore fluctuations in heat transport by examining the ensemble of Q_τ , the net heat exchange between the baths and the system, occurring within the time interval τ . We then construct the probability distribution function by generating histograms, as explained in Sec. II. In simulations, we test different values for τ , from 1 to 10 picoseconds, and separately study heat exchange at either the hot or cold contacts, as well as the behavior of the averaged heat exchanged.

Fig. 5 summarizes the analysis of the fluctuation data. In Fig. 5(a) we illustrate how the probability distribution func-

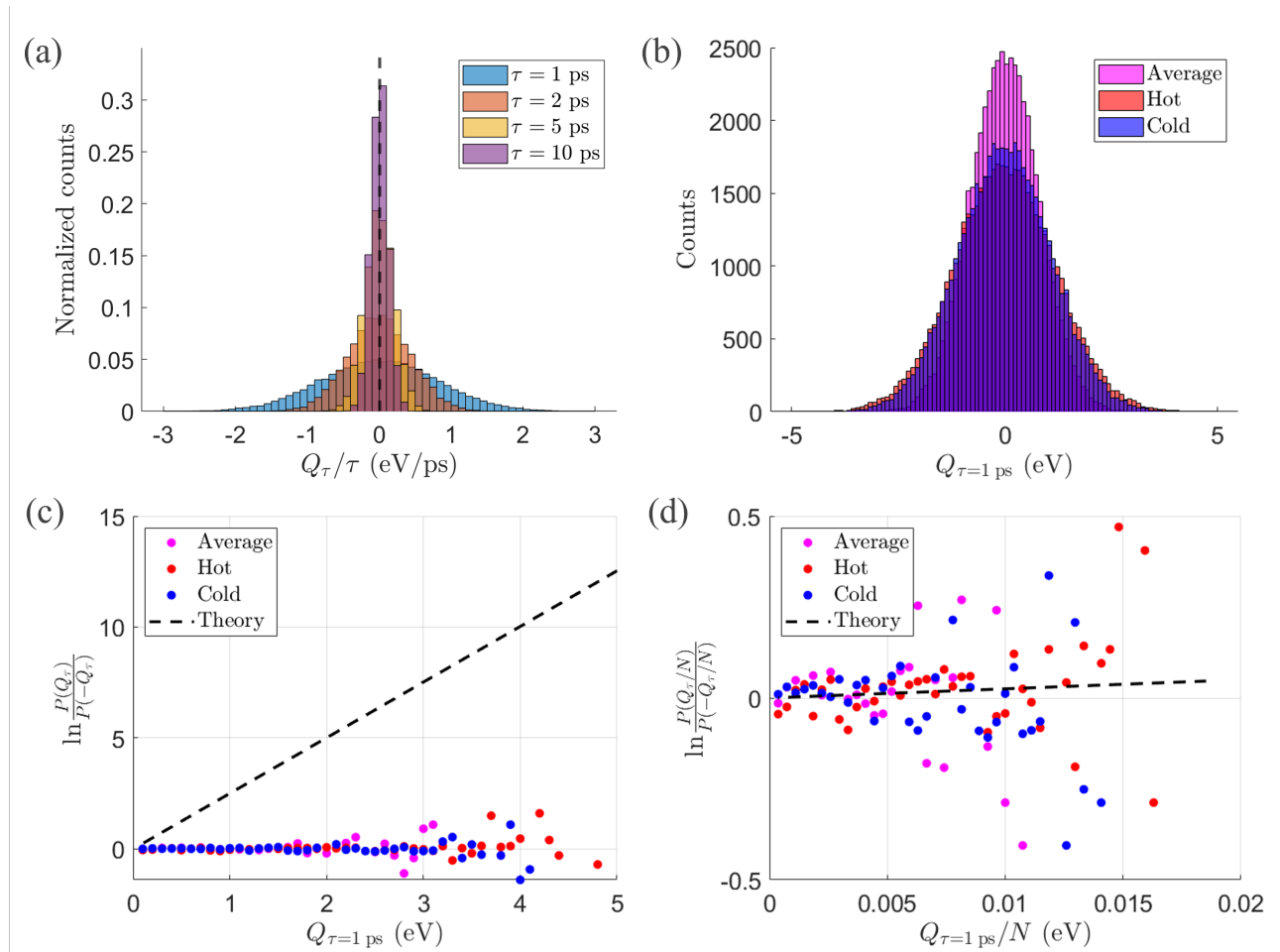


Figure 5. Testing the fluctuation symmetry in many-atom thermostats. (a) Histograms of integrated heat currents Q_τ^{ave}/τ with varying time interval τ . The black dotted line marks the value of the mean heat current J . (b) Overlaid histograms of integrated heat currents from individual baths, Q_τ^{hot} and Q_τ^{cold} , and Q_τ^{ave} with $\tau = 1$ ps. The histograms contain 50,000 data points for 50 ns simulation time, with $\tau = 1$ ps being the lowest time interval between each data points. (c), (d) Fluctuation symmetry plot with (c) Q_τ and (d) Q_τ/N , where $N = 270$ Au atoms coupled to thermostat on one end. Dashed lines indicate the theoretical $\Delta\beta = 2.5 \text{ eV}^{-1}$. Simulation parameters are imposed temperatures $T_{\text{hot}} = 310$ K and $T_{\text{cold}} = 290$ K, with $\Delta T_{\text{Au-Au}} \approx 20$ K, $\gamma^{-1} = 0.04$ ps.

tion evolves as a function of the inspected time interval τ . Note that upon increasing τ , we have fewer data points available for the analysis. Plotting the histogram against Q_τ/τ , the distributions become narrower as τ increases, but the positions of the average remain fixed. We extract from Fig. 5(a) the mean heat current, which is approximately 0.005 eV/ps , or $\approx 800 \text{ pW}$. This value gives the expected thermal conductance $G = 40 \text{ pW/K}$ with $\Delta T_{\text{Au-Au}} \approx 20 \text{ K}$.

In Fig. 5(b), we compare the probability distribution functions calculated at the hot and cold ends, denoted by Q_τ^{hot} and Q_τ^{cold} , respectively, along with a histogram generated by averaging the heat exchange process, Q_τ^{ave} . We find that the distribution generated from Q_τ^{hot} is slightly wider than that created from Q_τ^{cold} . However, the mean heat currents for these different histograms are identical. To test the heat exchange fluctuation symmetry, Eq. (1), we investigate the ratio $\ln[P(Q_\tau)/P(-Q_\tau)]$ for each of the three sets, presented in Fig. 5(c). Remarkably, results dramatically deviate from

the expected slope of $\Delta\beta$. Instead, each histogram behaves as almost an equilibrium distribution, and it does not reflect the nonequilibrium heat exchange process taking place. We attribute this failure of the NEMD simulations to respect the fluctuation symmetry to several issues:

1. *Choice of the integrator:* The velocity Verlet integrator employed by LAMMPS to solve the Langevin equation is not suitable for solving stochastic differential equations. Rather, it treats the random force on an equal footing as deterministic atomic forces. This in turn leads to substantial errors when using the interface definition for heat current Eq. (2) as discussed in Ref. 41. Other studies noted related problems in the velocity-Verlet or other common MD integrators resulting in difficulties generating correct equilibrium properties. Revisions to the standard velocity-Verlet scheme were implemented in LAMMPS, by coupling the deterministic and stochastic forces⁶⁵. These modified schemes generate the correct Boltzmann distribution^{65–67} and satisfy the Green-Kubo

relation⁶⁸. However, we tested the scheme of Ref. 65 and found that it did not resolve the fluctuation symmetry issue we observed with many-atom thermostats, and it produced results that were similar in trends to Fig. 5(c).

In addition, LAMMPS provides a method for calculating heat flux through the molecule (in a vector form) by computing the energy and stress tensor between interacting atoms⁶¹. This method still did not produce the correct fluctuation symmetry while introducing further ambiguities, such as in the estimation of the molecular length and in choosing the directionality of heat transport, resulting in an incorrect estimate for the average current.

2. *Definition of heat current:* As we demonstrated in Ref. 41 on a one-dimensional model system, the "interface" heat current definition, Eq. (2), is difficult to converge to the correct result, unlike an "internal" definition that counts the amount of energy exchanged from internal, interatomic interactions. Moreover, we showed in Ref. 41 that while the internal definition for heat exchange obeyed the fluctuation symmetry, even with a rough time step, the definition (2) in practice dissatisfied this symmetry, and even when the averaged currents converged to the correct value.

We emphasize that mathematically, there is nothing wrong with Eq. (2). Rather, as we showed in Ref. 41 this expression is slower to converge to the long time limit than the internal definition as one reduces the time step. The interface definition is also extremely sensitive to the integrator used and how exactly the stochastic force is evaluated, showing violations to the fluctuation symmetry even at very small timesteps⁴¹.

3. *Many-atom thermostats:* We further suspect that the application of many thermostats at each side, contributes to the generation of an effective local equilibrium at those ends, rather than a true nonequilibrium steady state. To probe this aspect, in Fig. 5(d) we test the fluctuation symmetry by scaling the heat, $\tilde{Q}_\tau = Q_\tau/N$, with $N = 270$ the number of thermostated atoms at each edge. Remarkably, the relationship $P(\tilde{Q}_\tau)/P(-\tilde{Q}_\tau) = e^{\Delta\beta\tilde{Q}_\tau}$ appears to hold for the scaled current. This rough observation motivates us to explore the transport behavior using *single-atom thermostats* as means to generate the correct statistics of heat exchange. This idea is developed and detailed in the next section.

IV. SINGLE-ATOM THERMOSTATS

A. Fluctuation symmetry

In an effort to generate data consistent with the fluctuation symmetry, we conduct simulations in which we implement single-atom thermostats. In this configuration, only a single atom on each side of the junction is coupled to the (hot or cold) thermostats. A graphical representation of this system is shown in Fig. 6 (a)-(b).

First, in Fig. 6(a), we illustrate the setup in which we thermalize a single gold atom at each side of the system, one towards a high temperature (310 K) and the other to a lower temperature (290 K). The temperature profile developing in the junction is displayed in Fig. 6(c). We note that the ac-

tual temperature bias is lower than 20 K, which is reasonable given the "gentle" nature of single-atom thermostats in this nonequilibrium (two-bath) setup. Calculating the actual temperature bias as developing on the gold section attached to the molecule we get $\Delta T_{\text{Au-Au}} = 10.8$ K.

The corresponding fluctuation symmetry (1) is examined in Fig. 7(a), and it is verified when compared to the theoretical curve with the generated $\Delta T_{\text{Au-Au}}$. In the Appendix, we study the heat exchange symmetry when evaluated at each contact. Notably, only once the heat is averaged over the two sides, as we do in Fig. 7(a), a single-atom thermostat provides data consistent with the fluctuation symmetry.

We also look at the case in which the thermostats are applied onto the sulfur atoms that contact the alkane chain to the gold, as shown in Fig. 6(b). The resulting temperature profile is displayed in Fig. 6(d) with $\Delta T_{\text{S-S}} = 16.7$ K. The fluctuation symmetry analysis for this configuration is presented in the Appendix for the individual baths, and in Fig. 7(b), once averaging heat exchange over the two baths. Note that when applying the thermostats directly onto the S atoms, we extract the molecular conductance characterizing the alkanedithiol chain, rather than the overall junction's conductance. The heat current is evaluated to be 0.0125 eV/ps. The calculation of the molecular conductance G_M using $\Delta T_{\text{S-S}}$ yields approximately 120 pW/K, which agrees with previous results³¹.

As for the fluctuation symmetry, in both applications of single-atom thermostats, either on a gold atom or on the sulfur, we find that it is obeyed when using the set Q_τ^{ave} . We further test the fluctuation symmetry for different time intervals, long enough to wash out initial conditions. We confirm in Fig. 7 that the fluctuation symmetry is valid irrespective of the chosen (long) time interval. Note however that we have a fixed-size set of 50,000 $\tau = 1$ ps data points. Using longer time intervals reduce the ensemble size, e.g., we have only 5,000 $\tau = 10$ ps data points.

It is important to emphasize that our construction of single-atom thermostats is not meant to suggest that this is how experiments are to be conducted. Rather, single-atom thermostats serve only as a *computational* device to address the shortcoming of the conventional NEMD simulation method. Its deficiencies stem from the improper solver and the heat current definition, exacerbated by having many atoms thermalized in conventional Langevin NEMD calculations.

In sum, conventional NEMD simulations as implemented in LAMMPS fail to reproduce data consistent with the heat exchange fluctuation symmetry. As an ad-hoc solution, we produced the correct statistics by (i) applying the cold and hot thermostats each on a single atom. (ii) Generating data after averaging the heat exchange at the two sides. A fundamental cure to this deficiency would be to use stochastic integrators and adopt a different definition of heat exchange: Rather than calculate it as a net heat exchange with the bath, evaluate the heat current across bonds, internally⁴¹.

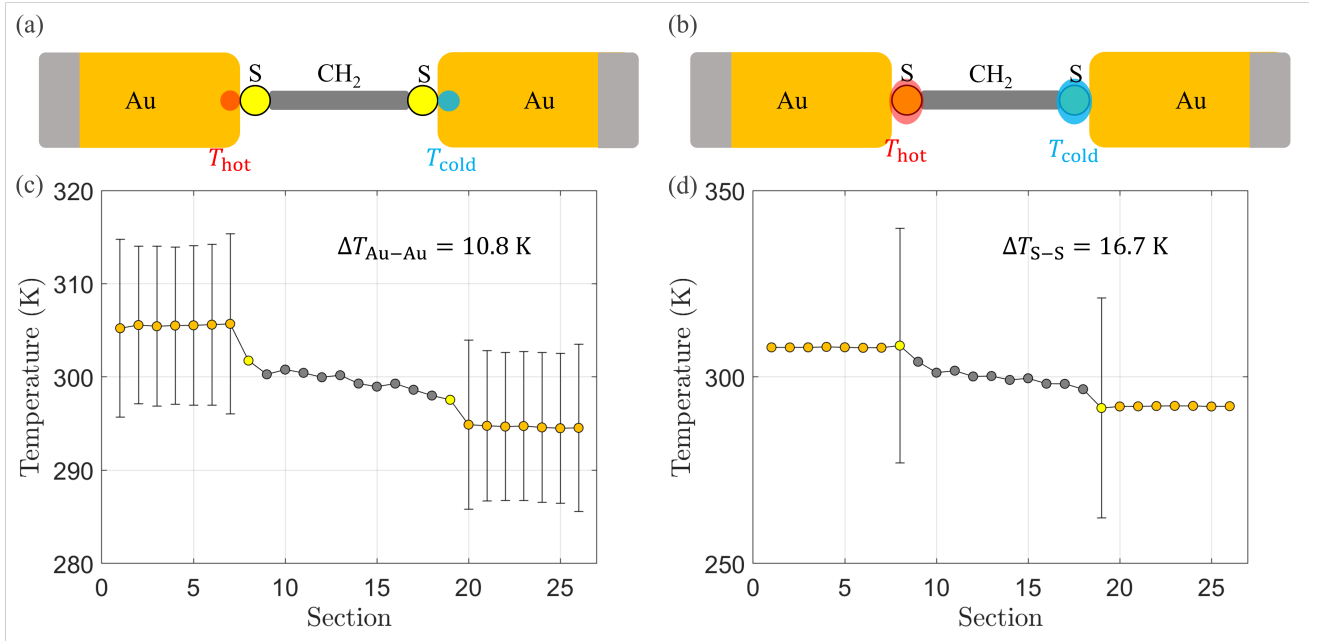


Figure 6. **Single-atom thermostats coupled to single atoms on both leads and the resulting temperature profile on the junction.** Illustration of thermostat positions are shown for (a) thermostats coupled to single Au atoms at the interface between lead and molecule, (b) thermostats coupled to single S atoms. (c), (d) Temperature profile plots of thermostat setups under respective illustrations. For both systems, simulation parameters are $\bar{T} = 300$ K, $\Delta T = 20$ K, $\gamma^{-1} = 0.04$ ps.

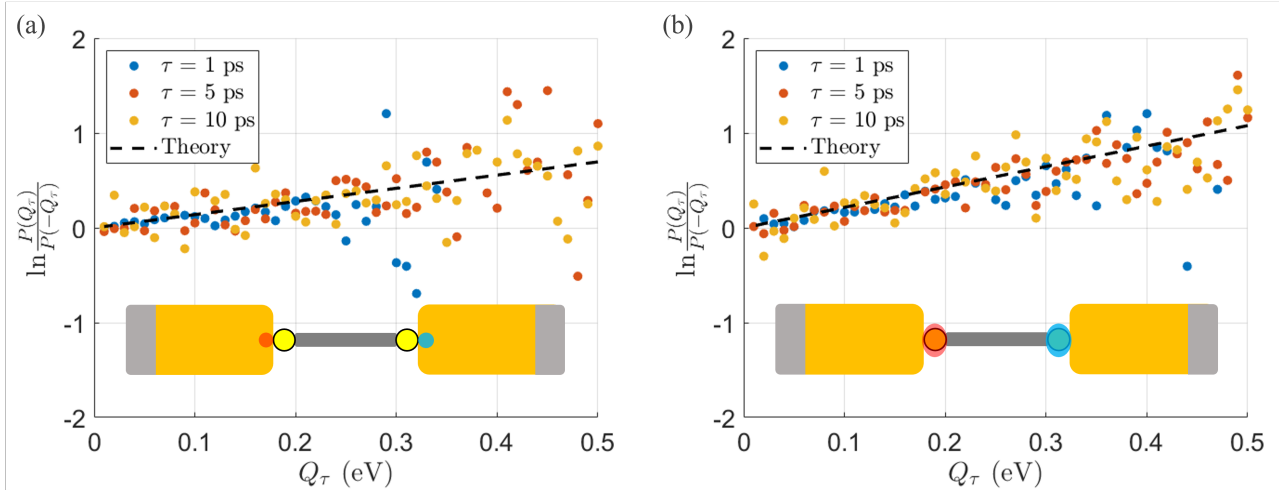


Figure 7. **Fluctuation symmetry analysis of Langevin thermostats coupled to single atoms on both leads.** (a) Fluctuation symmetry plot with a single gold atom thermalized at each side. The dashed line depicts the theoretical prediction with the slope $\Delta\beta = 1.39$ eV $^{-1}$. (b) Same, but thermalizing the S atoms at the ends of the alkane chain. The dashed line depicts the theoretical linear prediction with the slope $\Delta\beta = 2.16$ eV $^{-1}$. For both systems, the distributions contain 50,000 $\tau = 1$ ps data points and each element is constructed as $Q_\tau^{\text{ave},(i)} = [Q_\tau^{\text{cold},(i)} + Q_\tau^{\text{hot},(i)}]/2$. Simulation parameters are $\bar{T} = 300$ K, $\Delta T = 20$ K, $\gamma^{-1} = 0.04$ ps.

B. Conductance and the TUR

In the previous subsection, we demonstrated that a single-atom thermostat allowed generating data that respected the fluctuation symmetry. Building upon this result, we employ such thermostats to compute the thermal conductance of both the junction and the molecular building block, and confirm

that they act properly. Furthermore, we study the behavior of the heat current and current noise as a function of temperature bias. Using the current cumulants, we also investigate the thermodynamic uncertainty relation⁵¹.

In the Table I we present calculations of the thermal conductance obtained from three approaches: (i) Many-atom thermostats, acting on remote segments of the gold (270 atoms) as

Table I. Table of thermal conductance values as extracted from different thermostat configurations

Imposed target (K)	ΔT	Thermostat setup	Measured $\Delta T_{\text{Au-Au}}$ (K)	Measured $\Delta T_{\text{S-S}}$ (K)	Averaged heat current J ($\times 10^{-3}$ eV/ps)	Junction thermal conductance G (pW/K)	Molecular thermal conductance G_M (pW/K)
20		Au atoms at ends	19.7	8.50	5.50	44.8	104
		Single Au atom	10.8	4.21	3.40	50.6	130
		Single S atom	15.8	16.7	12.5	-	120
50		Au atoms at ends	47.5	16.1	13.0	43.7	129
		Single Au atom	28.2	10.5	7.50	42.3	114
		Single S atom	40.2	45.2	31.4	-	111
80		Au atoms at ends	74.3	25.1	19.5	42.1	125
		Single Au atom	45.0	15.6	12.2	43.5	126
		Single S atom	61.6	64.1	50.0	-	125

illustrated in Fig. 1. (ii) Single-atom thermostat applied onto a single gold atom placed next to the molecule. (iii) Single-atom thermostat, acting on the S atoms thus directly on the molecule. Note that this latter approach does not allow for the calculation of the junction's thermal conductance, G .

We find that the different methods yield consistent results for the thermal conductance, particularly when the imposed temperature bias is large. In contrast, when the imposed bias is small, the resulting $\Delta T_{\text{Au-Au}}$ is even smaller, and relative errors in the calculation increase. Overall, we conclude that single-atom thermostats are a suitable tool for calculating the thermal conductance of molecular junctions.

In Fig. 8, we study the behavior of the heat current, its noise, and the TUR as a function of temperature bias. These results were obtained by studying the set Q_τ^{ave} . First, in Fig. 8(a) we present the average current, computed by averaging over the ensemble of Q_τ and dividing it by the time interval considered, which varies from 1 ps to 10 ps. We find that the current remains the same across these different choices of time intervals, manifesting that the time interval is sufficiently long to achieve steady state.

Next, we turn in Fig. 8(b) to the second cumulant of $P(Q_\tau)$, denoted as $\langle\langle Q_\tau^2 \rangle\rangle = [\langle Q_\tau^2 \rangle - \langle Q_\tau \rangle^2]$. The current noise, or the scaled fluctuations of heat exchange $\langle\langle Q_\tau^2 \rangle\rangle/\tau$ is shown to approach a constant value with τ when τ is on the order of 10 ps.

Finally, we probe in Fig. 8(c) the TUR inequality,

$$\frac{\langle\langle Q_\tau^2 \rangle\rangle}{\langle Q_\tau \rangle^2} \frac{\langle \sigma_\tau \rangle}{k_B} \geq 2, \quad (4)$$

with $\langle \sigma_\tau \rangle$ as the cumulative entropy production during the time interval τ , which is long enough for steady state to set in. This dissipation-precision inequality translates to

$$\Delta\beta \frac{\langle\langle Q_\tau^2 \rangle\rangle}{\langle Q_\tau \rangle} \geq 2 \quad (5)$$

for heat transport problems as we study here. The relationship (5) has been proved for certain classes of models and dynamics: Continuous time Markov state process⁵², overdamped Langevin dynamics^{54,55}, and fully harmonic models⁵⁶. It was

also examined experimentally in Ref. 60, displaying violations to Eq. (5) due to quantum non-Markovian effects. While previous studies examined the TUR in simplified model systems, this relationship has rarely been assessed with realistic atomistic simulations⁶⁹. Specifically, it has not been studied in a physical molecular junction setup including realistic-anharmonic interactions, which we do here. Moreover, since Langevin thermostats act here on a single atom, the dynamics maintains inertial effects, thus it cannot be captured by overdamped equations.

In Fig. 8(c), we display the TUR ratio, corresponding to the left-hand side of Eq. (5), for several values of τ . Close to equilibrium, the TUR ratio appears to approach the expected value of 2. However, with an increasing temperature bias, we observe that the TUR ratio first increases, but then saturates, yet obeying the inequality in Eq. (5). Despite the fact that the heat current displays a linear dependence on the temperature bias even in the far-from-equilibrium regime, the second cumulant may gain nontrivial dependence on $\Delta T_{\text{Au-Au}}$ as it grows. As such, the overall behavior is not necessarily characterized by linear response, accounting for the TUR's departure from its expected value of 2. Note that using the Green-Kubo relation, $S_{\text{eq}} = \frac{J}{\Delta T} 2k_B T^2$, with S_{eq} the equilibrium noise, we find that for thermal conductance around 44 pW/K, the equilibrium noise should be 4.2×10^{-3} eV²/ps. Fig. 8(b) shows higher values, indicating additional contributions due to the nonequilibrium situation, as is further evidenced by the TUR value exceeding two.

Altogether, our simulations indicate that the TUR trade-off is satisfied in this real-life model for a molecular junction within the examined temperature range, which is relevant for experiments.

C. Experimental relevance

The time interval considered in Fig. 7(a) was in the 1-10 ps range with a temperature difference of about 10 degrees, $\Delta\beta \approx 1.4$ eV⁻¹. This translates to currents in the 0.003 eV/ps range (see Table I). Considering a heat exchange event with $Q_\tau = 0.2$ eV, we find that $P(Q_\tau)/P(-Q_\tau) \approx 1.3$. Thus, we ex-

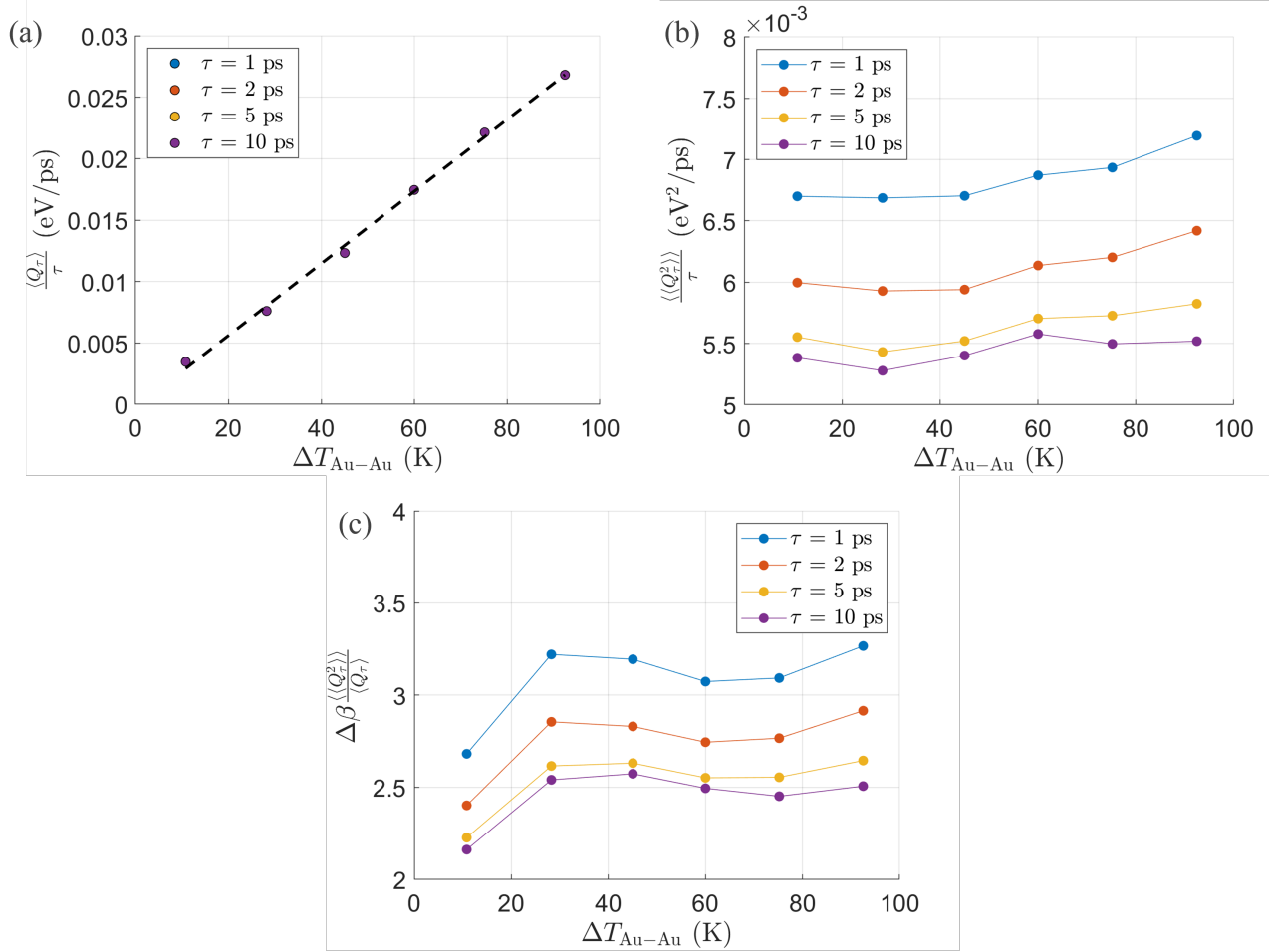


Figure 8. **Heat current and its noise with single-atom thermostats.** Data is plotted against the temperature difference developing between Au interface at the boundary of the molecule, $\Delta T_{\text{Au-Au}}$. **(a)** Averaged heat current, $\langle Q_\tau \rangle / \tau$ (data overlapping), **(b)** heat current variance, $\langle\langle Q_\tau^2 \rangle\rangle / \tau$ and **(c)** the TUR ratio, for which theoretical TUR ratio is greater or equal to 2. Results were generated from the ensemble $Q_\tau^{\text{ave},(i)}$ and are presented when using several different time intervals, τ .

pect that one should frequently-enough observe negative entropy production at this amount. However, time resolution is limited experimentally. Let us now assume that heat exchange is probed in time intervals of nanoseconds. Recall that approximately, the heat current in our system is 3 eV/ns for $\Delta T_{\text{Au-Au}} = 10$ K (see Fig. 7(a)). Within a ns time interval, a typical measurement would be in the $Q_\tau = 10$ eV range (see Fig. 2), translating into $P(Q_\tau)/P(-Q_\tau) = 4 \times 10^5$. Thus, if the time resolution in measurements is in nanoseconds, tens of millions of experiments would be required in our system in order to observe an instance of heat exchange against the temperature bias. Even more so, for a fluctuation at the amount of 20 eV, the ratio of probabilities exceeds 10^{11} . Note that increasing the averaged temperature, e.g., using $T_{\text{hot}} = 610$ and $T_{\text{cold}} = 590$ K, allows stronger fluctuations that facilitate data collection towards analyzing the fluctuation symmetry.

With measurements of heat exchange and its statistics in single-molecule junctions being extremely challenging, the role of simulations as we undertake in this study becomes even more important, serving to guide such efforts. As a first step,

our work here focused on the assessment and development of fitting computational tools.

V. SUMMARY

In this work, we studied the statistics of heat exchange using an atomistic description for a nanojunction. We noted the challenge of satisfying the fluctuation symmetry within conventional computational methods, and suggested a solution to produce physical data for the heat current noise.

We utilized the conventional nonequilibrium molecular dynamics approach as implemented in LAMMPS, where segments of the metal contact are thermally controlled by Langevin baths. While this standard approach yields the correct behavior for the averaged current and the thermal conductance, we showed that it failed to generate the correct statistics of heat exchange.

Our solution involved the implementation of single atom thermostats, acting on single atoms at each boundary, and

the additional averaging of heat exchange from the hot and cold edges. This ad-hoc approach successfully generated data that was consistent with the fluctuation symmetry. Additionally, these calculations of thermal conductance were consistent with other established methods. From the calculation of the second cumulant of heat exchange we were able to examine the thermodynamic uncertainty relation, which we showed to hold in the alkane molecular junction.

It was proved in Ref. 56 that the thermodynamic uncertainty relation (5) universally holds for harmonic systems in the steady state limit. In our study, the force field includes anharmonic interactions. For example, the S-Au bond is treated as a Morse potential, nonbonding interactions are handled with the Lennard-Jones potential, and dihedral terms are included within the molecule. However, at room temperature, heat transport in Au-alkane-Au chains is dominated by harmonic interactions resulting in ballistic transport^{22,29}. As such, the observation that the TUR is obeyed in our system, as displayed in Fig. 8, is not surprising. It is intriguing to probe the TUR in highly anharmonic junctions, in the underdamped dynamical limit, to assess its applicability in anharmonic systems.

Classical MD simulations are an effective tool for capturing the interatomic anharmonic force field. However, quantum effects become important when vibrational molecular modes and substrate phonons are of a higher frequency than the thermal energy. To treat, e.g., molecular junctions attached to Graphene electrodes, semiclassical methods were developed, incorporating quantum statistics into the modified Langevin equation^{29,70–72}. Extending our work, it is important to test whether such hybrid simulation approaches respect the universal entropy production fluctuation symmetry both analytically and numerically.

In future work we plan to investigate the thermal conductance and noise properties of more complex molecules, employing ab-initio MD or machine learning force fields rather than empirical potentials. However, clearly, future studies of current noise with molecular simulators require implementing robust and rigorous stochastic solvers and heat current calculations. Once implemented, noise calculations will assist the design of robust and optimal thermal devices such as thermal conductors, insulators, diodes, and refrigerators.

ACKNOWLEDGMENTS

DS acknowledges support from an NSERC Discovery Grant and the Canada Research Chairs program. The work of MG was supported by an NSERC Canada Graduate Scholarship—Doctoral (CGSD). We acknowledge Longji Cui for discussions that motivated this work.

AUTHOR DECLARATIONS

Conflict of Interest

The authors have no conflicts to disclose

DATA AVAILABILITY

The data that support the findings of this study are available from the corresponding author upon reasonable request.

APPENDIX: FLUCTUATION SYMMETRY FOR SINGLE-ATOM THERMOSTATS

This Appendix discusses Fig. 9, complementing Fig. 7. We use here the single-atom Au thermostat. We generate a set of Q_τ , build the full probability distribution function $P(Q_\tau)$, and then test the fluctuation symmetry, separately for heat exchange data collected at the hot and cold baths. While these results should be identical, we do find in Fig. 9 that the statistics at the two baths is different. However, we also build the histogram of the averaged heat exchanged at the two bath, $Q_\tau^{\text{ave},(i)} = [Q_\tau^{\text{cold},(i)} + Q_\tau^{\text{hot},(i)}]/2$. As we show in Fig. 7 in the main text, this combined data more closely follows the fluctuation ratio line.

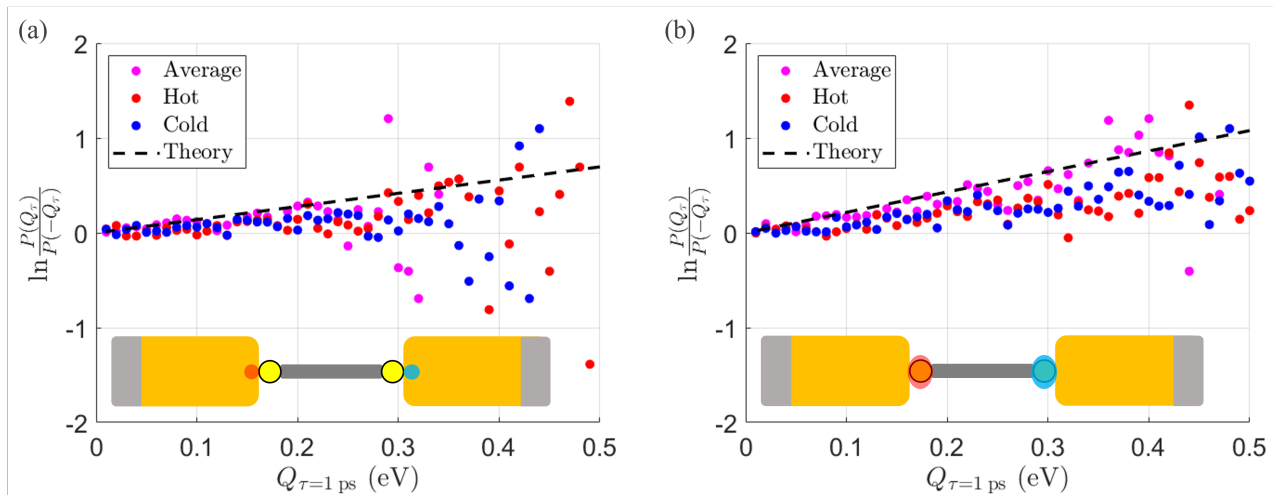


Figure 9. Fluctuation symmetry plots shown for (a) thermostats coupled to single Au atoms and (b) thermostats coupled to S atoms; the thermostats setups follow Fig. 6. The analysis here is completed for individual baths, Q_τ^{hot} and Q_τ^{cold} , in addition to Q_τ^{ave} using $\tau = 1$ ps. The results are processed from the same distributions as in Fig. 6-7, with simulation parameters $\bar{T} = 300$ K, $\Delta T = 20$ K, $\gamma^{-1} = 0.04$ ps.

REFERENCES

- E. Pop, "Energy dissipation and transport in nanoscale devices," *Nano Res.* **3**, 147 (2010).
- N. Li, J. Ren, L. Wang, G. Zhang, P. Hänggi, and B. Li, "Colloquium: Phononics: Manipulating heat flow with electronic analogs and beyond," *Rev. Mod. Phys.* **84**, 1045 (2012).
- T. Luo and G. Chen, "Nanoscale Heat Transfer - from Computation to Experiment," *Phys. Chem. Chem. Phys.* **15**, 3389 (2013).
- D. G. Cahill, P. V. Braun, G. Chen, D. R. Clarke, S. Fan, K. E. Goodson, P. Keblinski, W. P. King, G. D. Mahan, A. Majumdar, H. J. Maris, S. R. Phillpot, E. Pop, and L. Shi, "Nanoscale thermal transport. II. 2003–2012," *Appl. Phys. Rev.* **1**, 011305 (2014).
- D. M. Leitner, "Quantum Ergodicity and Energy Flow in Molecules," *Adv. Phys.* **64**, 445 (2015).
- D. Segal and B. K. Agarwalla, "Vibrational Heat Transport in Molecular Junctions," *Ann. Rev. Phys. Chem.* **67**, 185 (2016).
- S. Park, J. Jang, H. Kim, D. I. Park, K. Kim, and H. J. Yoon, "Thermal conductance in single molecules and self-assembled monolayers: physico-chemical insights, progress, and challenges," *J. Mater. Chem. A* **8**, 19746 (2020).
- Y. Li, W. Li, T. Han, X. Zheng, J. Li, B. Li, S. Fan, and C.-W. Qiu, "Transforming heat transfer with thermal metamaterials and devices," *Nat. Rev. Mater.* **6**, 488 (2021).
- J. Chen, X. Xu, J. Zhou, and B. Li, "Interfacial thermal resistance: Past, present, and future," *Rev. Mod. Phys.* **94**, 025002 (2022).
- B. Gotsmann, A. Gemma, and D. Segal, "Quantum phonon transport through channels and molecules—A Perspective," *App. Phys. Lett.* **120**, 160503 (2022).
- R. Y. Wang, R. A. Segalman, and A. Majumdar, "Room temperature thermal conductance of alkanedithiol self-assembled monolayers," *Appl. Phys. Lett.* **89**, 173113 (2006).
- Z. Wang, J. A. Carter, A. Lagutchev, Y. K. Koh, N.-H. Seong, D. G. Cahill, and D. D. Dlott, "Ultrafast Flash Thermal Conductance of Molecular Chains," *Science* **317**, 787 (2007).
- M. D. Losego, M. E. Grady, N. R. Sottos, D. G. Cahill, and P. V. Braun, "Effects of chemical bonding on heat transport across interfaces," *Nat. Mater.* **11**, 502 (2012).
- T. Meier, F. Menges, P. Nirmalraj, H. Hölscher, H. Riel, and B. Gotsmann, "Length-Dependent Thermal Transport along Molecular Chains," *Phys. Rev. Lett.* **113**, 060801 (2014).
- S. Majumdar, J. A. Sierra-Suarez, S. N. Schifres, W.-L. Ong, C. F. Higgins III, A. J. H. McGaughey, and J. A. Malen, "Vibrational Mismatch of Metal Leads Controls Thermal Conductance of Self-Assembled Monolayer Junctions," *Nano Lett.* **15**, 2985 (2015).
- S. Majumdar, J. A. Malen, and A. J. H. McGaughey, "Cooperative Molecular Behavior Enhances the Thermal Conductance of Binary Self-Assembled Monolayer Junctions," *Nano Lett.* **17**, 220 (2017).
- L. Cui, S. Hur, Z. A. Akbar, J. C. Klöckner, W. Jeong, F. Pauly, S.-Y. Jang, P. Reddy, and E. Meyhofer, "Thermal conductance of single-molecule junctions," *Nature* **572**, 628 (2019).
- N. Mosso, H. Sadeghi, A. Gemma, S. Sangtarash, U. Drechsler, C. Lambert, and B. Gotsmann, "Thermal Transport through Single-Molecule Junctions," *Nano Lett.* **19**, 7614 (2019).
- A. Gemma, F. Tabatabaei, U. Drechsler, A. Zulji, H. Dekkiche, N. Mosso, T. Niehaus, M. R. Bryce, S. Merabia, and B. Gotsmann, "Full thermoelectric characterization of a single molecule," *Nat. Commun.* **14**, 3868 (2023).
- A. Dhar, "Heat transport in low-dimensional systems," *Adv. Phys.* **57**, 457 (2008).
- G. Benenti, S. Lepri, and R. Livi, "Anomalous Heat Transport in Classical Many-Body Systems: Overview and Perspectives," *Front. Phys.* **8**, 292 (2020).
- D. Segal, A. Nitzan, and P. Hänggi, "Thermal conductance through molecular wires," *J. Chem. Phys.* **119**, 6840 (2003).
- K. Sasikumar and P. Keblinski, "Effect of chain conformation in the phonon transport across a Si-polyethylene single-molecule covalent junction," *J. Appl. Phys.* **109**, 114307 (2011).
- J. C. Klöckner, M. Bürkle, J. C. Cuevas, and F. Pauly, "Length dependence of the thermal conductance of alkane-based single-molecule junctions: An ab initio study," *Phys. Rev. B* **94**, 205425 (2016).
- J. C. Klöckner, J. C. Cuevas, and F. Pauly, "Transmission eigenchannels for coherent phonon transport," *Phys. Rev. B* **97**, 155432 (2018).
- R. Moghaddasi Fereidani and D. Segal, "Phononic heat transport in molecular junctions: Quantum effects and vibrational mismatch," *J. Chem. Phys.* **150**, 024105 (2019).
- M. Dinpajoo and A. Nitzan, "Heat conduction in polymer chains with controlled end-to-end distance," *J. Chem. Phys.* **153**, 164903 (2020).
- I. Sharony, R. Chen, and A. Nitzan, "Stochastic simulation of nonequilibrium heat conduction in extended molecular junctions," *J. Chem. Phys.* **153**, 144113 (2020).
- G. Li, B.-Z. Hu, N. Yang, and J.-T. Lü, "Temperature-dependent thermal transport of single molecular junctions from semiclassical Langevin molecular dynamics," *Phys. Rev. B* **104**, 245413 (2021).
- M. Dinpajoo and A. Nitzan, "Heat conduction in polymer chains: Effect of substrate on the thermal conductance," *J. Chem. Phys.* **156**, 144901 (2022).
- J. J. Wang, J. Gong, A. J. H. McGaughey, and D. Segal, "Simulations of heat transport in single-molecule junctions: Investigations of the thermal

- diode effect," *J. Chem. Phys.* **157**, 174105 (2022).
- ³²J. C. Klöckner and F. Pauly, "Variability of the thermal conductance of gold-alkane-gold single-molecule junctions studied using ab-initio and molecular dynamics approaches," [arXiv:1910.02443](https://arxiv.org/abs/1910.02443).
- ³³D. J. Evans, E. G. D. Cohen, and G. P. Morriss, "Probability of second law violations in shearing steady states," *Phys. Rev. Lett.* **71**, 2401 (1993).
- ³⁴S. Lepri, R. Livi, and A. Politi, "Energy transport in anharmonic lattices close to and far from equilibrium," *Physica D* **119**, 140 (1998).
- ³⁵D. J. Searles and D. J. Evans, "Fluctuation Theorem for Heat Flow," *Int. J. Thermophys.* **22**, 123 (2001).
- ³⁶C. Jarzynski, "Classical and Quantum Fluctuation Theorems for Heat Exchange," *Phys. Rev. Lett.* **92**, 230602 (2004).
- ³⁷K. Saito and A. Dhar, "Fluctuation Theorem in Quantum Heat Conduction," *Phys. Rev. Lett.* **99**, 180601 (2008).
- ³⁸D. J. Evans, D. J. Searles, and S. R. Williams, "On the probability of violations of Fourier's law for heat flow in small systems observed for short times," *J. Chem. Phys.* **132**, 024501 (2010).
- ³⁹U. Seifert, "Stochastic thermodynamics, fluctuation theorems and molecular machines," *Rep. Prog. Phys.* **75**, 126001 (2012).
- ⁴⁰S. Ciliberto, R. Gomez-Solano, and A. Petrosyan, "Fluctuations, Linear Response, and Currents in Out-of-Equilibrium Systems," *Ann. Rev. Condens. Matter Phys.* **4**, 235 (2013).
- ⁴¹N. Kalantar, B. K. Agarwalla, and D. Segal, "On the definitions and simulations of vibrational heat transport in nanojunctions," *J. Chem. Phys.* **153**, 174101 (2020).
- ⁴²L. Nicolin and D. Segal, "Non-equilibrium spin-boson model: Counting statistics and the heat exchange fluctuation theorem," *J. Chem. Phys.* **135**, 164106 (2011).
- ⁴³L. Nicolin and D. Segal, "Quantum fluctuation theorem for heat exchange in the strong coupling regime," *Phys. Rev. B* **84**, 161414 (2011).
- ⁴⁴D. Segal, "Heat transfer in the spin-boson model: A comparative study in the incoherent tunneling regime," *Phys. Rev. E* **90**, 012148 (2014).
- ⁴⁵C. Wang, J. Ren, and J. Cao, "Nonequilibrium Energy Transfer at Nanoscale: A Unified Theory from Weak to Strong Coupling," *Sci. Rep.* **5**, 11787 (2015).
- ⁴⁶J. Cerrillo, M. Buser, and T. Brandes, "Nonequilibrium quantum transport coefficients and transient dynamics of full counting statistics in the strong-coupling and non-Markovian regimes," *Phys. Rev. B* **94**, 214308 (2016).
- ⁴⁷B. K. Agarwalla and D. Segal, "Energy current and its statistics in the nonequilibrium spin-boson model: Majorana fermion representation," *New J. Phys.* **19**, 043030 (2017).
- ⁴⁸M. Kilgour, B. K. Agarwalla, and D. Segal, "Path-integral methodology and simulations of quantum thermal transport: Full counting statistics approach," *J. Chem. Phys.* **150**, 084111 (2019).
- ⁴⁹E. Aurell, B. Donvil, and K. Mallick, "Large deviations and fluctuation theorem for the quantum heat current in the spin-boson model," *Phys. Rev. E* **101**, 052116 (2020).
- ⁵⁰X. Cao, C. Wang, H. Zheng, and D. He, "Quantum thermal transport via a canonically transformed Redfield approach," *Phys. Rev. B* **103**, 075407 (2021).
- ⁵¹A. C. Barato and U. Seifert, "Thermodynamic uncertainty relation for biomolecular processes," *Phys. Rev. Lett.* **114**, 158101 (2015).
- ⁵²T. R. Gingrich, J. M. Horowitz, N. Perunov, and J. L. England, "Dissipation bounds all steady-state current fluctuations," *Phys. Rev. Lett.* **116**, 120601 (2016).
- ⁵³P. Pietzonka, A. C. Barato, and U. Seifert, "Universal bounds on current fluctuations," *Phys. Rev. E* **93**, 052145 (2016).
- ⁵⁴A. Dechant and S. Sasa, "Current fluctuations and transport efficiency for general Langevin systems," *J. Stat. Mech.: Theory Exp.* **2018**, 063209 (2018).
- ⁵⁵A. Dechant, "Multidimensional thermodynamic uncertainty relations," *J. Phys. A: Math. Theor.* **52**, 035001 (2019).
- ⁵⁶S. Saryal, H. M. Friedman, D. Segal, and B. K. Agarwalla, "Thermodynamic uncertainty relation in thermal transport," *Phys. Rev. E* **100**, 042101 (2019).
- ⁵⁷U. Seifert, "From Stochastic Thermodynamics to Thermodynamic Inference," *Annu. Rev. Condens. Matter Phys.* **10**, 171 (2019).
- ⁵⁸T. V. Vu and Y. Hasegawa, "Uncertainty relations for underdamped Langevin dynamics," *Phys. Rev. E* **100**, 032130 (2019).
- ⁵⁹J. M. Horowitz and T. R. Gingrich, "Thermodynamic uncertainty relations constrain non-equilibrium fluctuations," *Nat. Phys.* **16**, 15 (2020).
- ⁶⁰S. Pal, S. Saryal, D. Segal, T. S. Mahesh, and B. K. Agarwalla, "Experimental study of the thermodynamic uncertainty relation," *Phys. Rev. Res.* **2**, 022044(R) (2020).
- ⁶¹A. P. Thompson, H. M. Aktulga, R. Berger, D. S. Bolintineanu, W. M. Brown, P. S. Crozier, P. J. in 't Veld, A. Kohlmeyer, S. G. Moore, T. D. Nguyen, R. Shan, M. J. Stevens, J. Tranchida, C. Trott, and S. J. Plimpton, "LAMMPS - a flexible simulation tool for particle-based materials modeling at the atomic, meso, and continuum scales," *Comp. Phys. Comm.* **271**, 10817 (2022).
- ⁶²A. Stukowski, "Visualization and analysis of atomistic simulation data with OVITO-the Open Visualization Tool," *Modelling Simul. Mater. Sci. Eng.* **18**, 015012 (2010).
- ⁶³T.-Q. Duong, C. Massobrio, G. Ori, M. Boero, and E. Martin, "Thermal resistance of an interfacial molecular layer by first-principles molecular dynamics," *J. Chem. Phys.* **153**, 074704 (2020).
- ⁶⁴T. Luo and J. R. Lloyd, "Non-equilibrium molecular dynamics study of thermal energy transport in Au-SAM-Au junctions," *J. Heat Mass Transf.* **53**, 1 (2010).
- ⁶⁵N. Grønbech-Jensen and O. Farago, "A simple and effective Verlet-type algorithm for simulating Langevin dynamics," *Mol. Phys.* **111**, 983 (2013).
- ⁶⁶N. Grønbech-Jensen, N. R. Hayre, and O. Farago, "Application of the G-JF Discrete-Time Thermostat for Fast and Accurate Molecular Simulations," *Comput. Phys. Commun.* **185**, 524 (2014).
- ⁶⁷N. Grønbech-Jensen, "Complete set of stochastic Verlet-type thermostats for correct Langevin simulations," *Mol. Phys.* **118**, e1662506 (2019).
- ⁶⁸L. F. G. Jensen and N. Grønbech-Jensen, "Accurate configurational and kinetic statistics in discrete-time Langevin systems," *Mol. Phys.* **117**, 2511 (2019).
- ⁶⁹S. A. M. Loos, S. Arabha, A. Rajabpour, A. Hassanalí, and É. Roldán, "Nonreciprocal forces enable cold-to-hot heat transfer between nanoparticles," *Sci. Rep.* **13**, 4517 (2023).
- ⁷⁰J. S. Wang, "Quantum Thermal Transport from Classical Molecular Dynamics," *Phys. Rev. Lett.* **99**, 160601 (2007).
- ⁷¹J.-T. Lü, B.-Z. Hu, P. Hedegård, and M. Brandbyge, "Semi-classical generalized Langevin equation for equilibrium and nonequilibrium molecular dynamics simulation," *Prog. Surf. Sci.* **94**, 21 (2019).
- ⁷²R. Chen, M. Dinpajoo, and A. Nitzan, "Quantum bath augmented stochastic nonequilibrium atomistic simulations for molecular heat conduction," *J. Chem. Phys.* **159**, 134110 (2023).